

Power Generation Demonstration of Electrostatic Vibrational Energy Harvester with Comb Electrodes and Suspensions Located in Upper and Lower Decks

Hiroaki Honma,^{1*} Hiroyuki Mitsuya,^{2,3} Gen Hashiguchi,³
Hiroyuki Fujita,⁴ and Hiroshi Toshiyoshi¹

¹Institute of Industrial Science, The University of Tokyo, 4-6-1 Komaba, Meguro-ku, Tokyo 153-8505, Japan

²Saginomiya Seisakusho, Inc. 3-8-2 Okubo, Shinjuku-ku, Tokyo 169-0072, Japan

³Department of Mechanical and Engineering, Shizuoka University, 3-5-1 Hamamatsu, Shizuoka 432-8011, Japan

⁴Advanced Research Laboratories, Tokyo City University, 8-9-18 Todoroki, Setagaya-ku, Tokyo 158-0082, Japan

(Received January 14, 2022; accepted March 2, 2022)

Keywords: IoT, MEMS, vibrational energy harvester, electret, miniaturization

In this paper, a vibrational energy harvester formed in a double-deck structure is presented. Comb electrodes covered with an electret skin are located in the active layer of a silicon on insulator (SOI) wafer, and suspensions are formed in the handle layer, thereby reducing the footprint to 62% of that of the previous model. For electrical interconnection between the SOI and handle layers, part of the SOI layer is formed into a cantilever that is designed to adhere to the substrate. When the device is mechanically excited by sinusoidal acceleration of 0.18 G (1 G = 9.8 m/s²), it generates a power of 13.2 μW, corresponding to a normalized power density (NPD) of 1.23 mW/cm³/G².

1. Introduction

The energy harvester is a vital component for an autonomous wireless sensor node that runs without a battery, thus avoiding the need to frequently change the battery.^(1–4) Among various environmental energy sources, mechanical vibrations have received increasing attention because of their reliable abundance in various locations,⁽⁵⁾ even when sunlight is not available. Research interest has recently focused on the development of small energy harvesters that effectively convert mechanical power into electrical output.

Microelectromechanical systems (MEMS)-type vibrational energy harvesters are usually composed of a suspended movable body and suspensions, and resonance is used to convert incoming small-amplitude oscillations into a large stroke of the suspended mass so that the enhanced mechanical velocity is converted into electrical current through mechano-electric transduction. Amongst various transducer mechanisms such as the piezoelectric, electrostatic, and electromagnetic types, we have chosen electrostatic induction current using an electret (or permanent electrical charge) to effectively convert mechanical vibration into electrical power.

*Corresponding author: e-mail: honma-hh@iis.u-tokyo.ac.jp
<https://doi.org/10.18494/SAM3785>

Owing to the relatively large mechano-electric coupling through the electrostatic force, the performance of an electret-type harvester can be tuned to the vibrational frequency range.^(6–13) More than 1 mW power in low-frequency (<300 Hz) and small-acceleration (<1 G = 9.8 m/s²) ranges has been reported.⁽¹⁴⁾ However, a large chip size is usually required because the electromechanical transduction mechanism requires long suspensions to obtain large vibratory strokes. For instance, comb electrodes of a few hundred microns are used in a typical layout but a comparable space should be reserved for the suspensions, resulting in a large space that does not contribute to power generation.

To overcome this problem, we have newly adopted a double-deck structure to allocate electret comb electrodes and elastic suspensions in the active and handle layers of a silicon on insulator (SOI) wafer, respectively. In this paper, the design and power generation performance of a double-deck electrostatic vibrational energy harvester are reported. This paper is based on extended results reported elsewhere.⁽¹⁵⁾

2. Design

The output power of a vibrational energy harvester is usually described using an analytical model called the velocity-damped resonant generator (VDRG).⁽¹⁶⁾ When the movable body of an electrostatic energy harvester oscillates at resonance, the maximum output power P_{max} can be expressed as⁽¹⁷⁾

$$P_{max} = (1/2) m \omega^3 X_{lim} y, \quad (1)$$

where m and ω are the movable body mass and resonant angular frequency, respectively. The resonant frequency is usually set at the dominant frequency of the incoming vibrations to effectively convert kinetic energy into electrical power. The oscillation stroke of the chip frame is denoted by y , which is the same as the magnitude of the ambient vibration. X_{lim} is the position of the mechanical limit, where the movable mass stroke is stopped within the chip. As is evident from Eq. (1), high-power vibrational energy harvesters require a sufficiently large chip footprint to admit the enhanced oscillation of the suspended mass. In addition, a large proportion of the chip area should be reserved to accommodate the suspensions, which are usually designed to be long, allowing the mass to be oscillated at a large stroke.

Figure 1 shows schematic images of the top and bottom sides of the conventional design. The constraining electrostatic force is reduced using the symmetric electrode structures, thereby allowing a large electrical potential of the electret, which is charged on the sidewalls of the comb fingers.⁽¹⁸⁾ In the conventional chip design, the suspensions and electrodes are located side by side in the active layer, making it difficult to reduce the footprint.

The new harvester structures based on the double-deck design are shown in Fig. 2. The electrodes and suspensions are split into the active and handle layers, respectively. To form the electrical interconnection between the two layers, a cantilever is formed as part of the electrical wiring in the active layer; it is intentionally brought into contact with the handle layer using the surface stiction after the sacrificial release.⁽¹⁹⁾ The cantilever is described as the “stiction bar” in

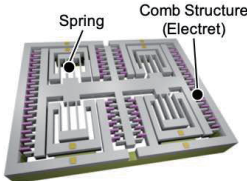
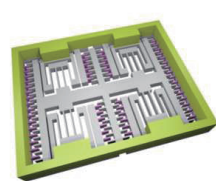
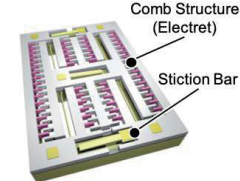
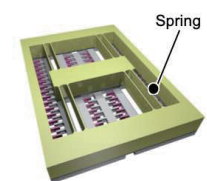
Conventional Energy-Harvester		Double-Deck Type Energy-Harvester	
Top Side (Active Layer of SOI)	Rear Side (Handle Layer of SOI)	Top Side (Active Layer of SOI)	Rear Side (Handle Layer of SOI)
			
Components in Top Side <ul style="list-style-type: none"> • Comb Electrodes • Springs 	Components in Rear Side <ul style="list-style-type: none"> • Not used 	Components in Top Side <ul style="list-style-type: none"> • Comb Electrodes • Stiction Bar (Elec. Connection) 	Components in Rear Side <ul style="list-style-type: none"> • Springs

Fig. 1. (Color online) Comparison of functional allocation schemes in the (a) conventional design and (b) this work. The conventional design uses the SOI layer for both the electrodes and the suspensions, while the new design splits them into a double-deck structure to reduce the chip area.

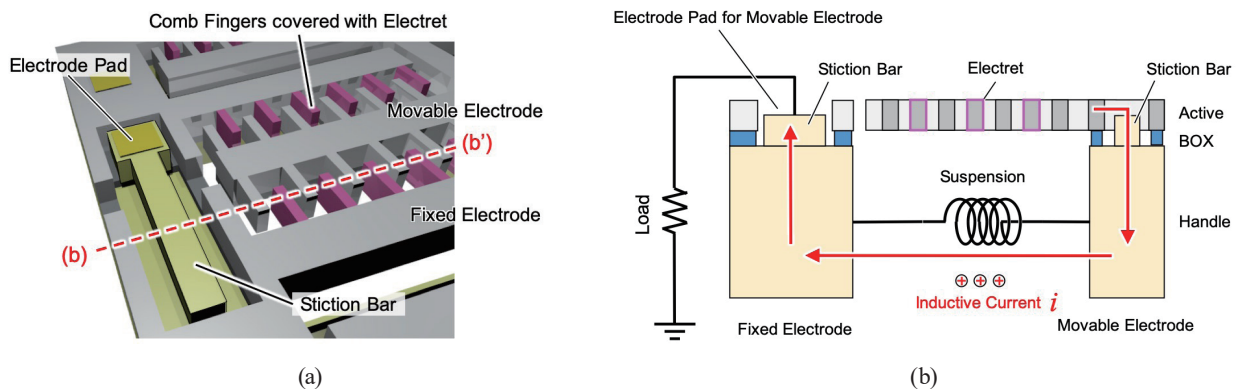


Fig. 2. (Color online) (a) Schematic and (b) cross-sectional views of the electrical interconnection between the electrode pad and the movable electrode. The stiction bars are brought into contact with the handle layer by the surface stiction, by which the movable electrodes are electrically connected to the electrical pad on the active layer through the suspensions formed in the handle layer.

Fig. 2(a). The electrical current generated in the SOI electrodes by the electrostatic induction is collected and transmitted through the suspensions in the handle layer, and delivered out from the contact pads. The chip footprint is thus significantly reduced while maintaining the generating power. Because of the double-deck structure, we have gained another degree of freedom in designing the mechanical rigidity of the suspension independently of the height of the electrodes.

3. Fabrication

A flow chart of the fabrication steps is shown in Fig. 3. An SOI wafer with a 100- μm -thick active layer, a 2- μm -thick buried oxide (BOX) layer, and a 500- μm -thick handle wafer is used. BOSCH-process deep reactive ion etching (DRIE) is used to define the patterns of the movable electrodes formed in the active layer. The handle layer of the wafer is also processed by DRIE to

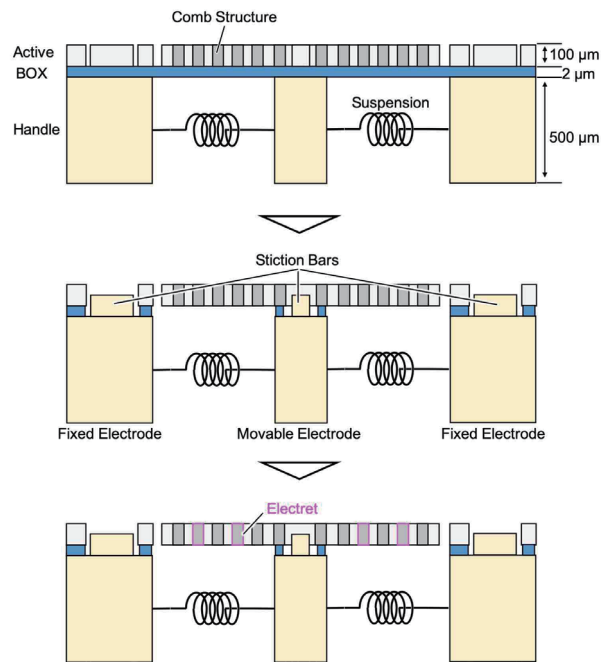


Fig. 3. (Color online) Flow chart of the fabrication steps of the vibrational energy harvester based on the electret comb electrodes and suspensions respectively located in the active and handle layers.

form a rigid block remaining on the back side of the suspended comb structure. Buffered hydrofluoric acid is used to selectively remove the BOX layer, and the movable structures are released. At the same time, the stiction bars in the active layer are intentionally brought into contact with the subjacent handle wafer by the surface stiction. The bars are also used as the electrical interconnection line between the upper and lower decks. Thereafter, a thermal oxide film is formed on the entire surface of the device by thermal oxidation. In this process, impurity atoms of potassium (K) are introduced into the silicon oxide using a water bubbler with potassium hydroxide (KOH). After the oxidation process, an electrical bias voltage of 250 V is applied to the comb electrodes for polarization at 500 °C; impurity ions (K^+) are driven out by the static field, after which the thermal oxide film becomes permanently charged as an electret layer (SiO^-) at -250 V with respect to the counter comb electrodes. Details of the manufacturing and charging processes for the electret film are reported elsewhere.^(20,21) When the external vibrations excite the movable mass and the electrodes, an electrostatic inductive current is produced by modulating the overlapping area between the comb fingers. The current is retrieved as the output through the stiction bars and the suspensions.

4. Experimental Results

SEM images of the harvester are shown in Figs. 4(a)–4(d). On the active layer side, almost the entire surface of the chip is filled with the comb electrodes, leaving the mechanical suspensions behind the active layer. Figure 4(b) shows the suspensions behind the active layer. We formed

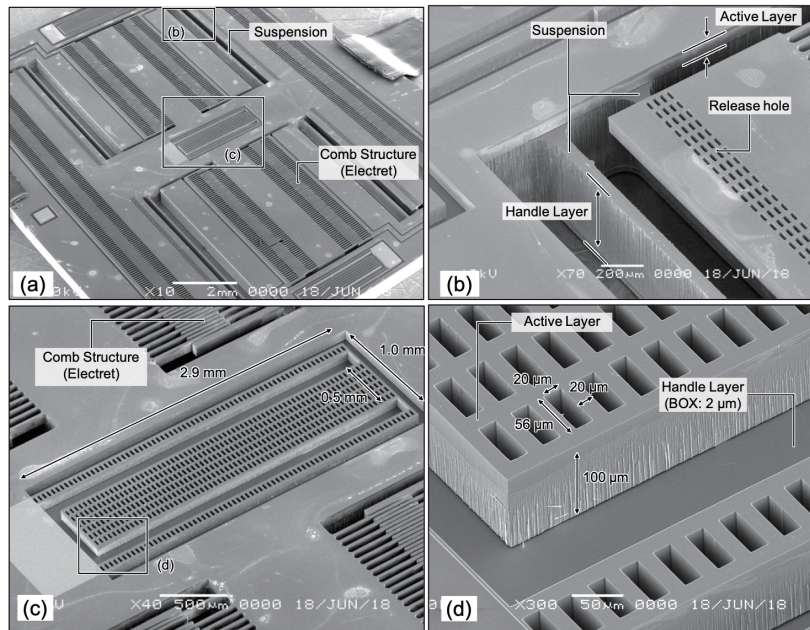


Fig. 4. SEM images of (a) harvester device with integrated electret comb structure and double-deck structure, (b) suspensions under the active layer of the SOI wafer, and (c and d) magnifications of part of the stiction bar.

release holes such that the suspensions would be free after the sacrificial release. Figures 4(c) and 4(d) show enlarged images of the stiction bar that acts as the electrical interconnection between the active and handle layers. The design parameters of the stiction bar are listed in Figs. 4(c) and 4(d). The bar is about 3 mm long, 0.5 mm wide, and 100 μm thick, with release holes at every 40 μm. Buffered hydrofluoric acid is introduced through the holes to etch the BOX layer. The bar is brought into contact during natural drying of rinse water. Here, a folded-beam structure is used to firmly adhere to the substrate. From SEM observation, we presume that the entire mesh structure at the tip of the holding bars is in contact with the substrate. The area around the stiction bar is used to mount an added metallic mass to save the device footprint.

Photographs of the conventional vibrational energy harvester (left) and the developed double-deck device (right) are shown in Fig. 5(a). The electrode pads shown in Fig. 5(b) are electrically connected to the movable electrode formed on the chip frame. The double-deck design reduces the chip area to $16 \times 13 \text{ mm}^2$ from the original dimensions of $20 \times 35 \text{ mm}^2$. In the case of 300 comb pairs, the area saved by the double-deck structure corresponds to 38% of that of the original design. Other design parameters are listed in Table 1.

A developed harvester was set on the shaker (Emic, 9514-AN/SD 373-A, DCS-98S Smart) to mechanically excite the movable electrode in the horizontal plane as shown in Fig. 6(a). A reference acceleration sensor was also attached to the vibration stage to construct a feedback system controlling the excitation acceleration. A high-speed microscope camera (Keyence, VW9000SP) was used to monitor the motion of the movable mass and the deformation of the suspension from an upright position. The output power was observed using the circuit shown in

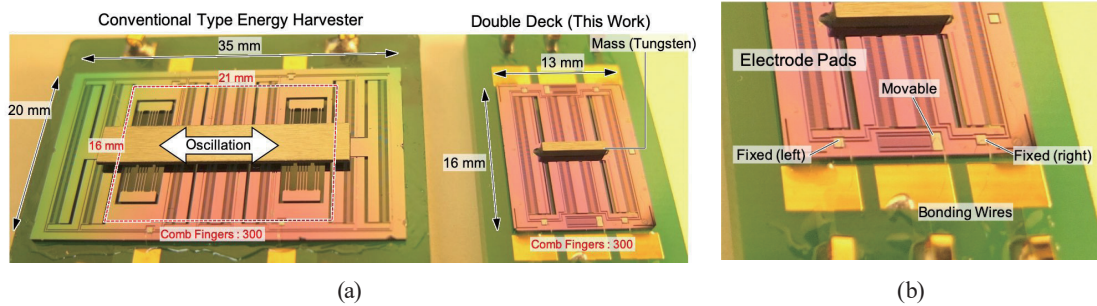


Fig. 5. (Color online) (a) Left: Photograph of the conventional design ($20 \times 35 \text{ mm}^2$). The electret comb structures and suspensions are arranged within the same plane. Right: Double-deck design ($16 \times 13 \text{ mm}^2$). (b) Close-up image of the electrode pads of the double-deck model.

Table 1
Design parameters of the conventional and new double-deck models.

	Conventional type	Double-deck type
Number of comb pairs	Total 900 pairs [300 pairs in area surrounded by red box in Fig. 5(a)]	300 pairs
Proof mass	1.5 g	0.3 g
Electret potential	-250 V	-250 V
Height of comb	100 μm	100 μm
Width of comb	20 μm	20 μm
Length of comb	700 μm	700 μm
Gap	14 μm	14 μm

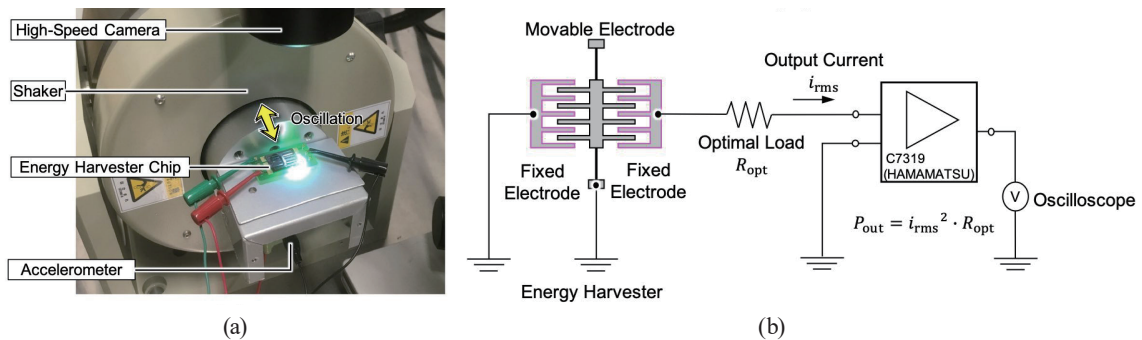


Fig. 6. (Color online) (a) Dynamic evaluation system for vibrational energy harvester and (b) power measurement circuit.

Fig. 6(b). The fixed electrode on the left was connected to the virtual ground of the current-voltage converter through a load resistance, while the one on the right was directly grounded.

Figure 7 shows snapshot images of the comb electrodes and the suspensions taken by the high-speed camera. The comb electrode was oscillated by sinusoidal waves with an acceleration of 0.12 G at 521 Hz. As is clear from the snapshot images, the elastic suspensions deployed under the active plate were deformed by the displacement of the movable electrode.

Figure 8 shows the observed waveforms of the short-circuit current. Although the device was oscillated under different vibration conditions, the waveform of the output current had a

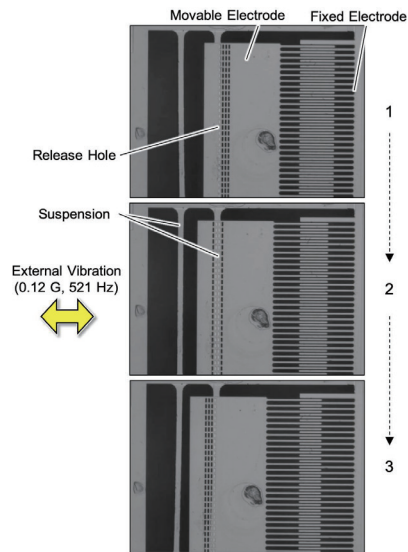


Fig. 7. (Color online) Snapshot images taken by the high-speed camera showing the operation of the comb electrode and suspensions under 0.12 G at 521 Hz.

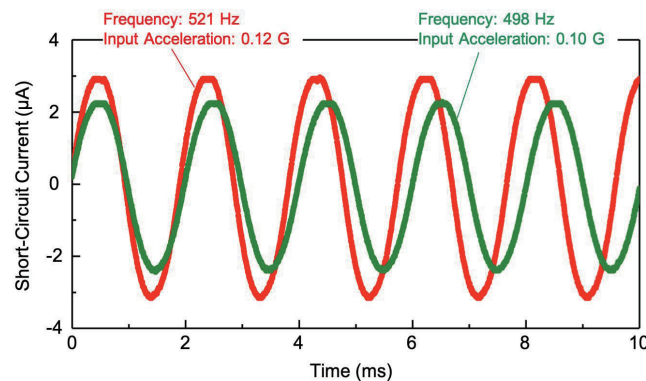


Fig. 8. (Color online) Short-circuit current waveform from the double-deck harvester when excited by sinusoidal vibration of 0.12 G at 521 Hz.

sinusoidal wave component at the same frequency as the external vibration. Peak values of ± 2.2 and ± 2.9 μA were observed when the amplitudes of the external vibration were 0.10 and 0.12 G, respectively. From the results, the double-deck structure was found to act as a vibrational energy harvester.

Figure 9(a) shows the amplitude of the short-circuit current as a function of the vibration frequency of the shaker. Chirped excitation vibrations from 0.01 to 0.13 G were used for this measurement. Since the spectrum was found to extend toward the higher frequency, we found that the device had a hard-spring effect in the vibrational frequency range between 459 and 525 Hz. The resonant frequency was designed at 480 Hz in good agreement with the

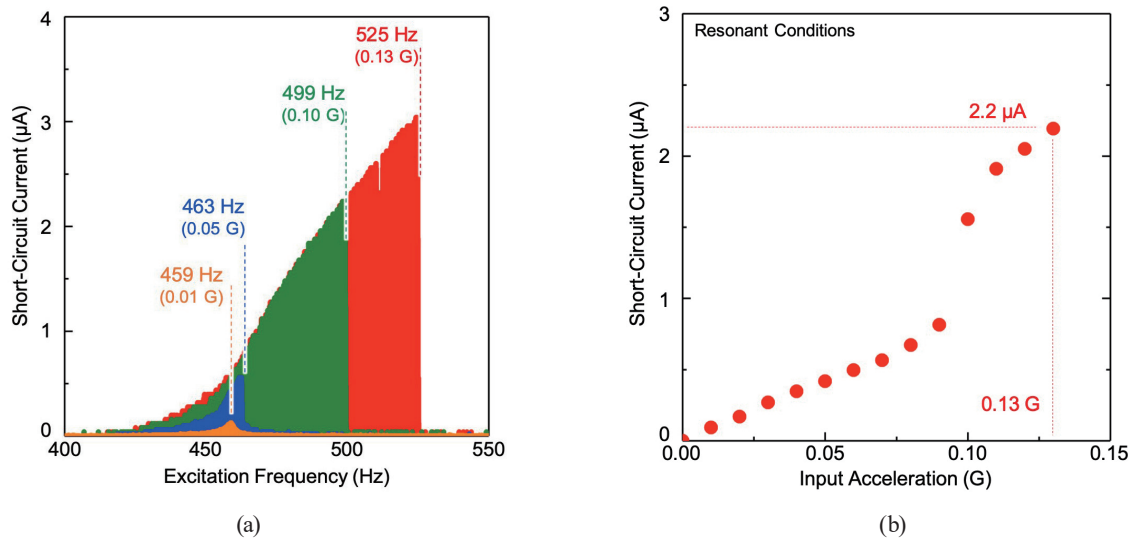


Fig. 9. (Color online) (a) Experimentally measured short-circuit currents under different acceleration conditions. Chirped excitation vibrations with constant amplitudes of acceleration from 0.01 to 0.13 G were used. (b) Short-circuit current under resonance as a function of excitation acceleration.

measurement; the frequency was chosen only for a proof-of-concept purpose. It could be tailored to be lower than 300 Hz corresponding to environmental vibrations using an extra tungsten mass of 0.45 g, corresponding to a volume of $1 \times 4 \times 6 \text{ mm}^3$. The root-mean-square value of the short-circuit current as a function of the excitation acceleration is shown in Fig. 9(b). The current becomes large with increasing acceleration, reaching 2.2 μA at 0.13 G.

The output power was measured as a function of the load resistance when the device was excited at its resonant frequency with a sinusoidal acceleration of 0.05 G, as shown in Fig. 10. The graph shows the optimal resistance of the developed double-deck device. As a result, a 5 M Ω resistor was found to be the optimal load at which the deliverable power was maximized.

The output power as a function of the acceleration when the device was excited and optimally loaded with a 5 M Ω resistor is shown in Fig. 11. An output power of 13.2 μW at 0.18 G was obtained. The power density normalized by the chip volume and input acceleration (NPD) was 1.23 $\text{mW}/\text{cm}^3/\text{G}^2$ at the input acceleration of 0.18 G. Nevertheless, the power in the small-acceleration range ($<0.11 \text{ G}$) remained small. A possible cause of this nonlinearity was the resistance of the electrical interconnection in the chip. The current–voltage characteristic between the fixed and movable electrodes was determined using a source meter (Keithley 2400), as shown in Fig. 12, in which Schottky diode characteristics were found. We suspect that the silicon–silicon contact between the stiction bar and the substrate had a non-ohmic nature that distorted the current–voltage curve and hence the power–acceleration curve.

Fixed and movable electrodes are usually connected for short-circuit measurement but our device had a Schottky diode element in the stiction bar. The short-circuit condition was thus affected by the Schottky barrier particularly in the small acceleration range ($<0.09 \text{ G}$), exhibiting a strong nonlinearity as shown in Fig. 9(b). This effect can be mitigated by lowering the intrinsic resistance of the stiction bar. An additional metallization on the sidewalls of the stiction bar to be used to lower the resistance to 100 Ω or less would also help, as reported elsewhere.⁽²²⁾

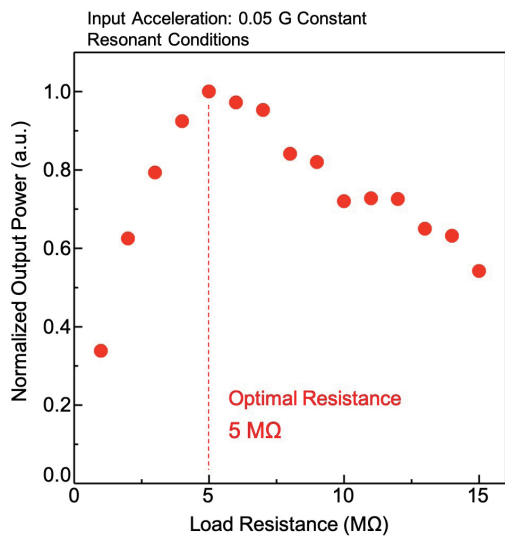


Fig. 10. (Color online) Output power normalized by peak value under different load resistances upon excitation by 0.05 G acceleration at resonance frequency.

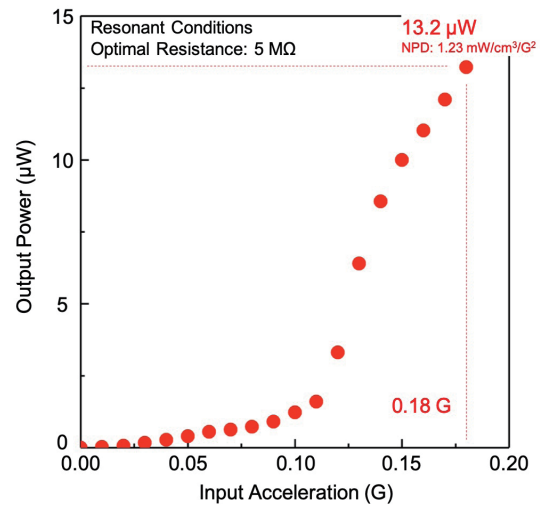


Fig. 11. (Color online) Output power as a function of the excitation acceleration, measured at the resonance frequency with the optimal load resistance of 5 MΩ.

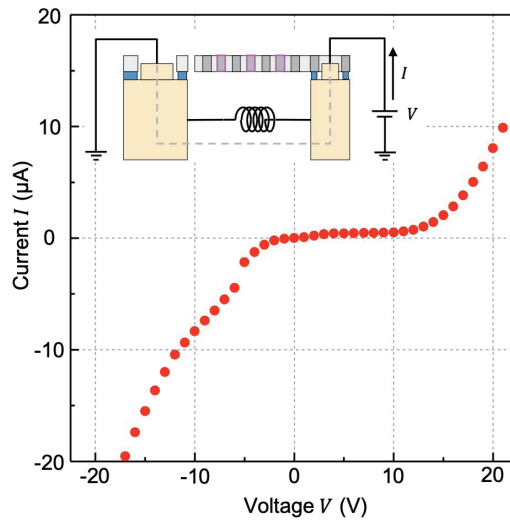


Fig. 12. (Color online) Experimentally measured current–voltage characteristic between the fixed and movable electrodes in the double-deck harvester, determined using a source meter (Keithley 2400).

5. Conclusions

A double-deck silicon structure was newly introduced to produce a MEMS vibrational energy harvester, where power-generating electrodes and elastic suspensions were respectively arranged in the active and handle layers and interconnected with a silicon stiction bar. Compared

with 300 comb electrode pairs, the device footprint saved by the double-deck structure corresponded to 38% of that of the original design, in which the electrodes and suspensions were flattened in a single layer. Despite the small footprint, energy harvester operation was experimentally confirmed, delivering an output power of 13.2 μ W for a sinusoidal waveform acceleration of 0.18 G at the resonant frequency 525 Hz. The device design is useful to make a compact autonomous power source for wireless sensor nodes.

Acknowledgments

This work was supported by JST CREST Grant Number JPMJCR15Q4 and by JSPS Grants-in-Aid for Scientific Research (B) (Grant Numbers 18H01490 and 19K15038).

References

- 1 L. Atzori, A. Iera, and G. Morabito: *Comput. Networks* **54** (2010) 2787. <https://doi.org/10.1016/j.comnet.2010.05.010>
- 2 S. Roundy, P. K. Wright, and J. Rabaey: *Comput. Commun.* **26** (2003) 1131. [https://doi.org/10.1016/S0140-3664\(02\)00248-7](https://doi.org/10.1016/S0140-3664(02)00248-7)
- 3 N. S. Hudak and G. G. Amatucci: *J. Appl. Phys.* **103** (2008) 101301. <https://doi.org/10.1063/1.2918987>
- 4 S. P. Beeby, M. J. Tudor, and N. M. White: *Meas. Sci. Technol.* **17** (2006) R175. <https://doi.org/10.1088/0957-0233/17/12/R01>
- 5 P. D Mitcheson, T. C. Green, E. M. Yetman, and A. S. Holmes: *J. Microelectromech. Syst.* **13** (2004) 429. <https://doi.org/10.1109/JMEMS.2004.830151>
- 6 Y. Zhang, T. Wang, A. Luo, Y. Hu, X. Li, and F. Wang: *Appl. Energy* **212** (2018) 362. <https://doi.org/10.1016/j.apenergy.2017.12.053>
- 7 C. P. Le and E. Halvorsen: *J. Micromech. Microeng.* **22** (2012) 074013. <https://doi.org/10.1088/0960-1317/22/7/074013>
- 8 K. Tao, J. Miao, S. W. Lye, and X. Hu: *Sens. Actuators, A* **228** (2015) 95. <https://doi.org/10.1088/0960-1317/25/10/104014>
- 9 N. Sato, K. Ono, T. Shimamura, K. Kuwabara, M. Ugajin, and Y. Sato: *J. Microelectromech. Syst.* **21** (2012) 1218. <https://doi.org/10.1109/JMEMS.2012.2204862>
- 10 T. Masaki, K. Sakurai, T. Yokoyama, M. Ikuta, H. Sameshima, M. Doi, T. Seki, and M. Oba: *J. Micromech. Microeng.* **21** (2011) 104004. <https://doi.org/10.1088/0960-1317/21/10/104004>
- 11 Y. Suzuki, D. Miki, M. Edamoto, and M. Honzumi: *J. Micromech. Microeng.* **20** (2010) 104002. <https://doi.org/10.1088/0960-1317/20/10/104002>
- 12 H. Koga, H. Mitsuya, H. Honma, H. Fujita, H. Toshiyoshi, and G. Hashiguchi: *MDPI Micromachines* **8** (2017) 293. <https://doi.org/10.3390/mi8100293>
- 13 H. Honma, Y. Tohyama, H. Mitsuya, G. Hashiguchi, H. Fujita, and H. Toshiyoshi: *J. Micromech. Microeng.* **29** (2019) 084002. <https://doi.org/10.1088/1361-6439/ab2371>
- 14 H. Honma, Y. Tohyama, H. Mitsuya, G. Hashiguchi, H. Fujita, and H. Toshiyoshi: *J. Micromech. Microeng.* **31** (2021) 125008. <https://doi.org/10.1088/1361-6439/ac2e46>
- 15 H. Honma and H. Toshiyoshi: *Proc. 2019 IEEE 32nd Int. Conf. Micro Electro Mechanical Systems (IEEE MEMS, 2019)* 1017. <http://doi.org/10.1109/MEMSYS.2019.8870642>
- 16 P. D. Mitcheson, E. M. Yeatman, G. K. Rao, A. S. Holmes, and T. C. Green: *Proc. THE IEEE* **96** (2008) 1457. <http://doi.org/10.1109/JPROC.2008.927494>
- 17 H. Toshiyoshi, S. Ju, H. Honma, C. -H. Ji, and H. Fujita: *Sci. Techno. Adv. Mater.* **20** (2019) 124. <https://doi.org/10.1080/14686996.2019.1569828>
- 18 H. Honma, H. Mitsuya, G. Hashiguchi, H. Fujita, and H. Toshiyoshi: *J. Micromech. Microeng.* **28** (2018) 064005. <https://doi.org/10.1088/1361-6439/aab514>
- 19 K. Takahashi, M. Mita, H. Fujita, and H. Toshiyoshi: *IEICE Electron. Express* **3** (2006) 197. <https://doi.org/10.1587/elex.3.197>
- 20 G. Hashiguchi, D. Nakanone, T. Sugiyama, M. Ataka, and H. Toshiyoshi: *AIP Adv.* **6** (2016) 035004. <https://doi.org/10.1063/1.4943528>

- 21 T. Nakanishi, T. Miyajima, K. Chokawa, M. Araidai, H. Toshiyoshi, T. Sugiyama, G. Hashiguchi, and K. Shiraishi: Appl. Phys. Lett. **117** (2020) 193902. <https://doi.org/10.1063/5.0029012>
- 22 K. Takahashi, M. Mita, H. Fujita, and H. Toshiyoshi: IEEE/ASME J. Microelectromech. Syst. **18** (2009) 818. <https://doi.org/10.1109/JMEMS.2009.2018371>

About the Authors



Hiroaki Honma received his M.E. and Ph.D. degrees in electrical engineering from Toyohashi University of Technology, Aichi, Japan, in 2013 and 2016, respectively. He joined the Institute of Industrial Science (IIS), The University of Tokyo in 2016 as a project researcher. Since 2020, he has been a project research associate with the IIS, The University of Tokyo. His research interests include optical MEMS, power MEMS, and CMOS-MEMS.

(honma-hh@iis.u-tokyo.ac.jp)



Hiroyuki Mitsuya received his B.S. degree from Seikei University, Tokyo, Japan, in 2002. He has been with Saginomiya Seisakusho, Inc., since 2002. He is currently involved in the investigation of electret MEMS.

(hiro-mitsuya@saginomiya.co.jp)



Gen Hashiguchi received his M.S. degree in electrical engineering from Chuo University, Tokyo, Japan, in 1988, and his Ph.D. degree in electrical engineering from The University of Tokyo, Tokyo, Japan, in 1996. From 1988 to 1998, he was with Nippon Steel Corporation, where he was involved with the development of micro devices, including thermal sensors, field emitters, and amorphous silicon imaging sensors. In 1999, he became a professor of mechanical engineering at Kagawa University, Kagawa, Japan, and in 2007, he joined the Research Institute of Electronics, Shizuoka University. His current research interests are MEMS with an emphasis on electret devices.

(hashiguchi.gen@shizuoka.ac.jp)



Hiroyuki Fujita is a professor of Tokyo City University and honorary director of the Advanced Research Laboratory of Canon Medical Systems Corporation. He is also professor emeritus of The University of Tokyo (UTokyo), where he served as a professor in the Institute of Industrial Science of UTokyo for over 38 years. He received his B.S., M.S., and Ph.D. degrees in electrical engineering from UTokyo in 1975, 1977, and 1980, respectively. He is currently engaged in the investigation of MEMS/NEMS for bio/nanotechnology and vibrational energy harvesters for IoT. (hfujita@tcu.ac.jp)



Hiroshi Toshiyoshi received his M.E. and Ph.D. degrees in electrical engineering from The University of Tokyo, Tokyo, Japan, in 1993 and 1996, respectively. He joined the Institute of Industrial Science (IIS), The University of Tokyo in 1996 as a lecturer. From 1999 to 2001, he was a visiting assistant professor at the University of California, Los Angeles, CA, USA. In 2002, he became an associate professor with the IIS, The University of Tokyo. From 2005 to 2008, he was the project leader of the Optomechatronics Project at Kanagawa Academy of Science and Technology, Kawasaki, Japan. Since 2009, he has been a professor with the IIS, The University of Tokyo. His research interests include optical and power MEMS. (hiro@iis.u-tokyo.ac.jp)